Effects of substrates, film thickness and temperature on thermal emittance of Mo/substrate deposited by magnetron sputtering

CrossMark

Yuping Ning [a], Wenwen Wang [a], Ying Sun [a], Yongxin Wu [a], Yingfang Liu [a], Hongliang Man [a], Muhammad Imran Malik [a], Cong Wang [a, b, *], Shuxi Zhao [c], Eric Tomasella [d], Angélique Bousquet [d]

[a] Center for Condensed Matter and Material Physics, Department of Physics, Beihang University, Beijing 100191, China
[b] Pneumatic and Thermodynamic Energy Storage and Supply Beijing Key Laboratory, Beijing, China
[c] Division of Solid State Physics, Ångström Laboratory, Uppsala University, Sweden
[d] Clermont Université, Université Blaise Pascal, Institute of Chemistry of Clermont-Ferrand (ICCF), CNRS-UMR 6296, 24 Avenue des Landais, 63171 Aubière, France

ABSTRACT

The thermal emittance of the Mo film, as an IR-reflector in solar selective absorbing coatings, is the most important property. The effects of the substrate material, the substrate surface roughness, the film thickness and the temperature on the thermal emittance of the Mo/substrate have been investigated. A series of Mo films with increasing film thickness were deposited on two types of substrate materials (glass and stainless steel). A saturated Mo thickness of 50 nm is found to produce the lowest thermal emittance. The thermal emittance of the Mo film is reduced by decreasing the substrate surface roughness. The emittance of the optimal Mo film remains 0.05 from 25 °C to 400 °C, which can meet the optical requirements for the IR-reflector.

© 2016 Elsevier Ltd. All rights reserved.

1. Introduction

Solar selective absorbing coating (SSAC) is designed to maximize photothermal conversion efficiency. Namely, it should maximally absorb solar radiation corresponding to blackbody radiation at 5777 K from 0.3 μm to 2.5 μm and minimally emit the infrared (IR) thermal radiation from 2.5 μm to 20 μm at working temperature (100 °C–400 °C) [1,2]. The thermal energy transferred from the absorbed solar energy is taken away by the heat transfer fluid for electric power application as shown in Fig. 1. Hence an ideal SSAC should both have a high solar absorptance α (close to one) in solar radiation range and a low thermal emittance ε (close to zero) in IR range. The typical double cermet coating structure from surface to substrate (steel tube in Fig. 1) consists of a ceramic anti-reflection layer, a low and a high metal volume fraction cermet solar absorption layers (LMVF and HMVF), and a metal IR-reflector layer [3] as shown in Fig. 2.

The performance for SSAC is characterized by the photothermal conversion efficiency [4] given in Eq. (1), which should be close to the maximum value one.

$$\eta_T = \alpha - \frac{\sigma T^4}{CI}\varepsilon_T \tag{1}$$

where α is solar absorptance, ε_T is the thermal emittance at temperature T of the SSAC, σ is the Stefan–Boltzmann constant $(5.67 \times 10^{-8}\,\mathrm{W/m^2\,K^4})$, I is the irradiance (typically 1000 W/m²) and C is solar concentration (for parabolic trough typically $C = 80$). Thus enhancing solar absorptance and suppressing thermal emittance are effective methods to improve the photothermal conversion efficiency according to Eq. (1). The solar absorptance for most SSACs [5–7] have approached to maximum value one, whereas it is difficult to decrease the thermal emittance of SSACs to zero. To improve the photothermal conversion efficiency, it is effective to reduce the thermal emittance of SSACs.

Reduction of thermal emittance of the metal IR-reflector layer is a crucial method to inhibit the thermal emittance of the SSAC [8]. The preparation parameters of the metal layer have an important effect on the emittance. The emittance is decreased with decrease
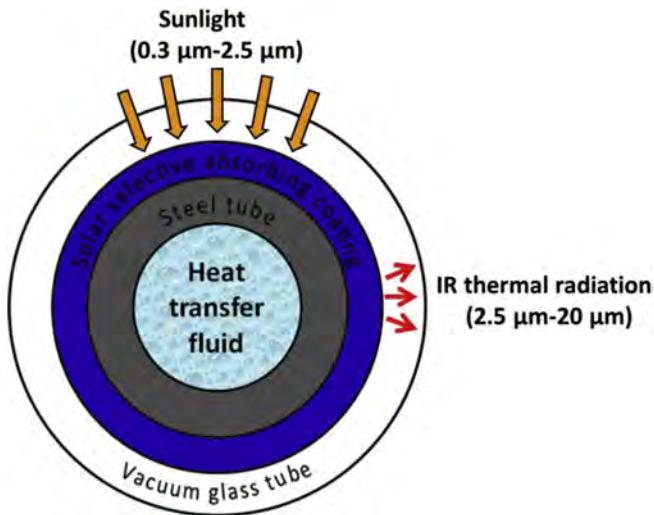

Fig. 1. Cross section of the receiver tube used in the parabolic trough collector (a kind of solar thermal collector).
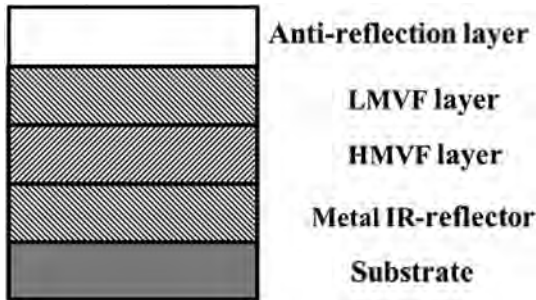

Fig. 2. Schematic diagram of the typical double cermet layer structure for SSAC.

in the sputtering gas pressure [9–13] and increase in the target power [14,15], due to the great change in the microstructure of the metal layer [9]. Thus, the low working gas pressure and high target power were used to prepare the metal IR-reflector in this paper. The recent results have shown that the emittance of the Au film and W film is reduced by decreasing the substrate surface roughness [16,17], which is also verified by the result in this paper.

The metal IR-reflector layer should have not only high reflectance in the IR range but also excellent thermal stability at elevated temperature. Molybdenum (Mo) possesses high melting point (2623 °C) among all the metals. In addition, the SSACs of NiAl-Al$_2$O$_3$ and Mo-SiO$_2$ used Mo films as IR-reflector have high thermal stability at 500 °C [18], 600 °C [19] and 800 °C [20] in vacuum respectively. Hence, high IR reflecting Mo is a promising candidate as an IR-reflector layer [7,21–23]. In addition, Mo is also used as a back contact and its optical properties are quite important in thin film solar cell community [12,13]. In this paper, the magnetron sputtering is used to deposit the Mo film [20,24,25] and stainless steel (SS) is selected as the substrate for the industrial production requirement. The effects of the substrate materials, substrate surface roughness, film thickness and temperature on the emittance of the Mo/substrate have been studied in detail. The SSAC of SiO$_2$/ZrSiON/ZrSiN/Mo is prepared, in which the optimized Mo film is used as the IR-reflector.

2. Experiments

Stainless steels 304 (304SS) and glass are used as substrates. The 3D parameter average roughness (Sa) is defined as the arithmetic mean of the absolute value of the deviation from the mean height [26], given by Eq. (2).

$$Sa = \frac{1}{MN} \sum_{i=1}^{M} \sum_{j=1}^{N} \left| z\left(x_i, y_j\right) - \mu \right| \tag{2}$$

Where $\mu = \frac{1}{MN} \sum_{i=1}^{M} \sum_{j=1}^{N} z(x_i, y_j)$ is the mean height. An equally spaced digitised 3D surface, can be denoted by z (x_i, y_j) ($x_i = i\Delta x$, $y_j = j\Delta y$; i = 1, 2, … M; j = 1, 2, … N), where Δx and Δy are the sampling intervals, and M and N represent the number of sampling points in the x and y directions, respectively. The values of Sa of all the substrates are listed in Table 1. The SS1, SS2 and SS3 denote the stainless steels with the polished surface, the specific treated surface and the sand blasting surface respectively. The surface treatment for the SS2 substrate includes four steps: cold rolling, heat treatment, acid pickling or dephosphorization, bright annealing. The Mo films with thickness range of 6–180 nm, 10–250 nm and 10–10000 nm were deposited on glass, SS1-2 and SS3 substrates by a JGP350C magnetron sputtering equipment as shown in Fig. 3 [24]. The size of Mo target is Φ60 mm × 4 mm with a purity of 99.95%. All substrates were cleaned with alcohol followed by de-ionized water in an ultrasonic agitator and blow-dried before being deposited. The detailed preparation parameters are listed in Table 2.

The thermal emittance for the opaque sample and semi-transparent sample is calculated according to Eq. (3) and Eq. (4), respectively [27]. Intensity distribution of the blackbody radiation at temperature from 25 °C to 400 °C is in the wavelength range of 1–100 μm, and the main intensity distributes in the wavelength range of 1–20 μm.

$$\varepsilon_{(25°C-400°C)} = \frac{\int_{1\mu m}^{100\mu m} (1 - R(\lambda)) I_b(\lambda, T) d\lambda}{\int_{1\mu m}^{100\mu m} I_b(\lambda, T) d\lambda} \tag{3}$$

$$\varepsilon_{(25°C-400°C)} = \frac{\int_{1\mu m}^{100\mu m} (1 - R(\lambda) - \tau(\lambda)) I_b(\lambda, T) d\lambda}{\int_{1\mu m}^{100\mu m} I_b(\lambda, T) d\lambda} \tag{4}$$

Where $I_b(\lambda, T)$ is the blackbody radiation at the given temperature T. Reflectance $R(\lambda)$ and transmittance $\tau(\lambda)$ are measured at normal incidence and room temperature. All samples are opaque except for the samples of 6–50 nm thick Mo films on glass substrate.

The solar absorptance (α) is weighted by the solar spectral radiation $I_s(\lambda)$ as shown in Eq. (5). The main solar energy (more than 95%) distributes from 0.3 μm to 2.5 μm.

Table 1
The surface average roughness (Sa) of all the substrates and the emittance (100 °C) of 50 nm Mo/substrate.

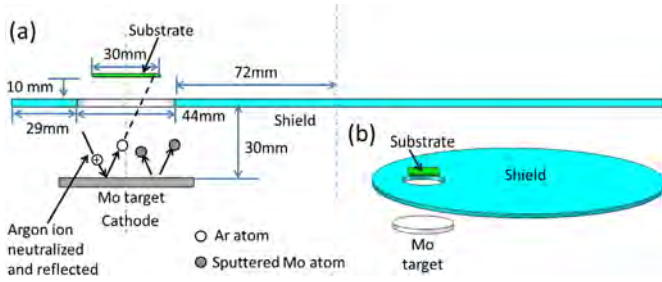| Substrates	SS1	Glass	SS2	SS3
Sa (nm) of substrate	1	3	23	1497
Emittance (100 °C) of 50 nm Mo/substrate	0.05	0.07	0.08	0.32

Fig. 3. Schematic (a) cross sectional and (b) three dimensional representations of the geometry of the magnetron sputtering system.

Table 2
The deposition parameters for the Mo films.

Sputtering method	Base vacuum	Substrate-to-target distance	Ar gas flow rate	Sputtering pressure	Power density
DC	1×10^{-3} (Pa)	40 (mm)	8.3×10^{-7} (m³/s)	0.4 (Pa)	5.9 (W/cm²)

$$\alpha = \frac{\int_{0.3\mu m}^{2.5\mu m} (1 - R(\lambda))I_S(\lambda)\mathrm{d}\lambda}{\int_{0.3\mu m}^{2.5\mu m} I_S(\lambda)\mathrm{d}\lambda} \quad (5)$$

Reflectance and transmittance in the wavelength range of 0.3–2.5 μm and reflectance in the wavelength range of 2.5–22 μm were measured by a Perkin-Elmer Lambda 900 UV/VIS/NIR double beam spectrometer and Fourier Transform Infrared Reflectance (FTIR) spectrometer Bruker Tensor 27, respectively. The other reflectance data in the wavelength range of 23–100 μm were extrapolated. Both instruments are equipped with the integrating sphere coated with BaSO₄ powder and gold respectively, for reducing diffuse scattering effect. An error of ±0.02 in the emittance values is adopted as same as that in the Zhao's result [28], because the same spectrometers and calculation method were used to get the emittance values in the present study. The surface morphologies of the Mo films on SS substrates were observed by a scanning electron microscopy (SEM). The Mo film thickness was measured using a Dektak 6M surface profiler. The surface roughness of the substrates was measured by the atomic force microscope (AFM) CSPM400 (for the smooth surface). For the SS3 substrate, the surface roughness was measured by the white light interferometer due to beyond the measurement range of the AFM.

3. Results and discussion

3.1. Effect of substrate material on emittance of Mo/substrate

The emittance variation of Mo films with increasing film thickness deposited on glass (Sa = 3 nm) and SS1 (Sa = 1 nm) substrates is shown in Fig. 4. The effect of the substrate material on the emittance of Mo/substrate depends on the film thickness. The emittance decreases sharply with film thickness (less than 50 nm) and keeps unchanged when the film thickness is greater than 50 nm. Here the film thickness value of 50 nm is defined as the saturated thickness. The thermal radiation of the substrate can't be suppressed when the film thickness less than the saturated thickness. The thermal radiation of the Mo/substrate comes from both the substrate and the Mo film. In addition, the emittance of the glass substrate (0.86) is considerably larger than that of the SS1 substrate (0.11). Hence, the emittance of Mo/glass is larger than that

of Mo/SS1 under the same film thickness (less than 50 nm). Furthermore, the contribution of substrate to the thermal radiation is becoming smaller as the film thickness increasing and when the saturated thickness is exceeded, the thermal radiation is all derived from the Mo film.

3.2. Effect of substrate surface roughness on emittance of Mo/substrate

The emittance of Mo films, which were deposited on the three stainless steel substrates with gradually increasing surface roughness, is shown in Fig. 5. The emittance is obviously suppressed by
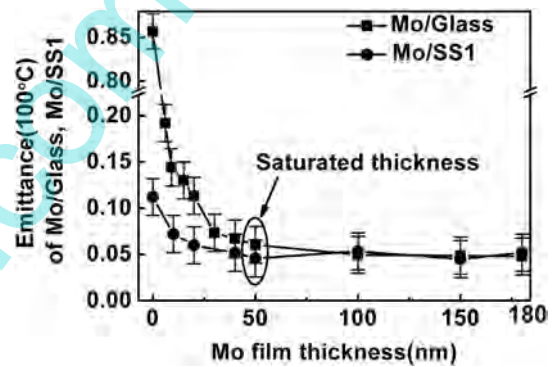

Fig. 4. Emittance variation of the Mo films with increasing thicknesses deposited on glass and SS1 substrates.

decreasing the substrate surface roughness under the same film thickness. As shown in Table 1, the emittance is 0.32, 0.08 and 0.05 for 50 nm thick Mo films on SS3, SS2 and SS1 respectively. It results from the enhanced reflectance of the Mo/substrate induced by decreasing substrate surface roughness as shown in Fig. 6.

The variations of reflectance and emittance are due to the different morphologies of Mo films on the SS1, SS2 and SS3 substrates as shown in Fig. 7 and Fig. 8. The morphologies of the three
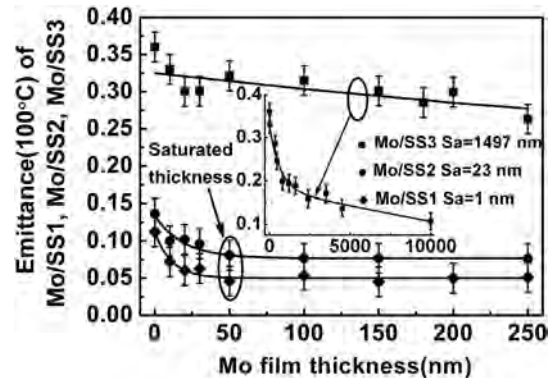

Fig. 5. Emittance variation of the Mo films with increasing thicknesses deposited on SS1, SS2 and SS3 substrates.
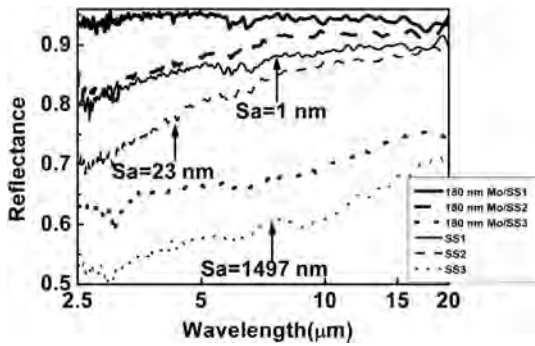
Fig. 6. Reflectance spectra of the Mo films and the corresponding SS1, SS2 and SS3 substrates.

absorbing more light [29–31]. Hence the reflectance of Mo films on SS2 and SS3 is lower than that of Mo film on SS1 in Fig. 6.

3.3. Effect of film thickness on emittance of Mo/substrate

The effect of film thickness on the emittance of Mo/substrate depends on the substrate surface roughness as shown in Fig. 5. There is a saturated thickness about 50 nm for Mo films deposited on SS1 (Sa = 1 nm) and SS2 (Sa = 23 nm) substrates. The emittance keeps the lowest value when the film thickness is larger than the saturated value, which is in accord with the results in literature [17,32]. However, there is not a saturated thickness for Mo films deposited on SS3 substrate. Due to the large surface roughness of SS3 substrate (Sa = 1497 nm), it is hardly to obtain a low emittance
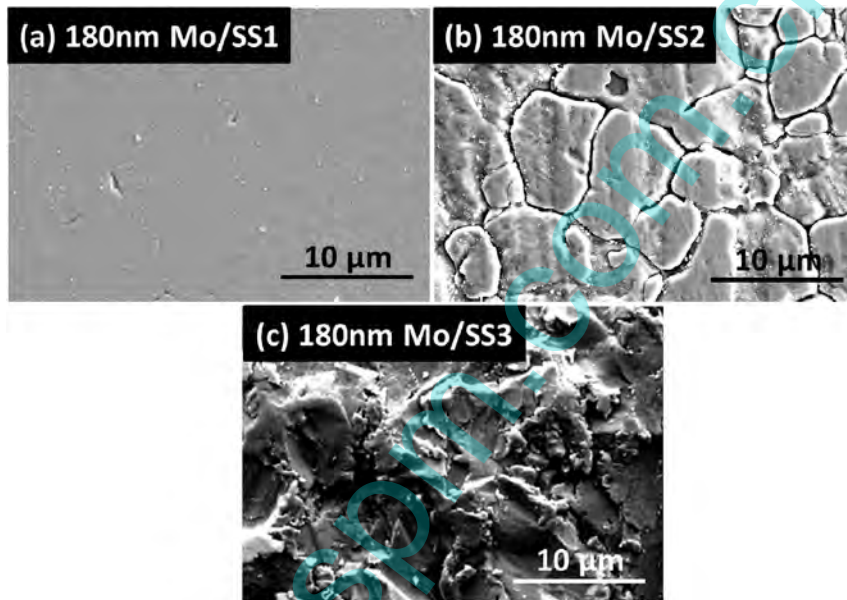

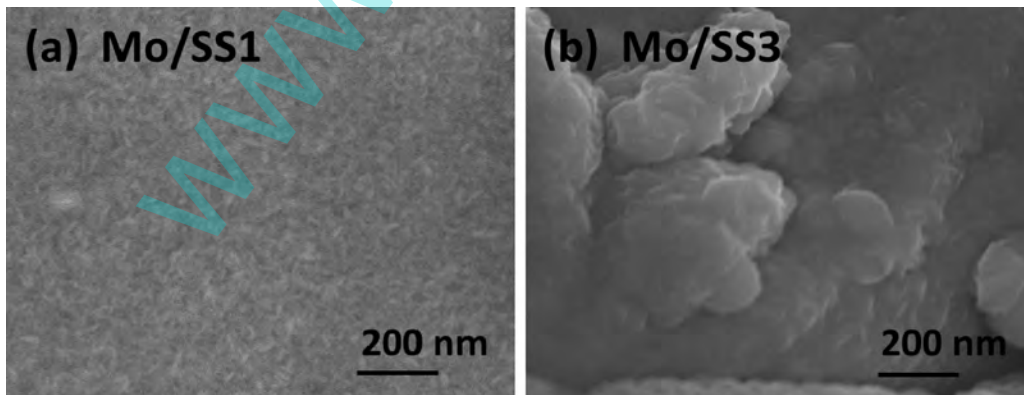**Fig. 7.** SEM morphologies of the Mo films on SS1, SS2 and SS3 substrates.

Fig. 8. SEM morphologies of the Mo films in nanometer scale on SS1 and SS3 substrates, (a) 180 nm Mo/SS1; (b) 250 nm Mo/SS3.

substrates remain unchanged although the substrates are covered by the Mo films. The surface of Mo film deposited on SS1 is smooth as shown in Fig. 7(a). However, the cloudy-like structures of Mo film on SS2 and the ravine-like structures of Mo film on SS3 are presented in Fig. 7(b) and (c), which forms optical traps for

for the Mo/SS3 despite the film thickness reaching 10 μm.

3.4. Effect of temperature on emittance of Mo/substrate

The emittance variations of the Mo films with calculated

temperature, deposited on SS1, SS2 and SS3 substrates, are shown in Fig. 9. The emittance increases monotonously with temperature for the Mo films on SS2 and SS3 substrates. However, it keeps 0.05 from 25 °C to 400 °C for the Mo films on SS1, which satisfies the optical requirements for the IR-reflector.

The emittance variations of the Mo films with calculated temperature on SS1, SS2 and SS3 result from their reflectance variations with wavelength. If

$$\int\limits_{1\mu m}^{100\mu m} I_b(\lambda, T)\mathrm{d}\lambda = c(T) \tag{6}$$

Eq. (7) is obtained via substituting Eq. (6) into Eq. (3), where the range of T is 25 °C–400 °C.

$$\varepsilon_T = \int\limits_{1\mu m}^{100\mu m} (1 - R(\lambda))\frac{I_b(\lambda, T)}{c(T)}\mathrm{d}\lambda = \int\limits_{1\mu m}^{100\mu m} (1 - R(\lambda))I'_b(\lambda, T)\mathrm{d}\lambda \tag{7}$$

Eq. (8) is obtained according to Eq. (7) and Eq. (6),

$$\int\limits_{1\mu m}^{100\mu m} I'_b(\lambda, T)\mathrm{d}\lambda = \int\limits_{1\mu m}^{100\mu m} \frac{I_b(\lambda, T)}{c(T)}\mathrm{d}\lambda = \frac{1}{c(T)}\int\limits_{1\mu m}^{100\mu m} I_b(\lambda, T)\mathrm{d}\lambda = 1 \tag{8}$$

According to Eq. (7), the emittance is the function of $(1-R(\lambda))$ and $I'_b(\lambda, T)$, where $I'_b(\lambda, T)$ is only determined by temperature when the wavelength is fixed. The $(1-R(\lambda))$ depends on the reflectance spectra $R(\lambda)$. The reflectance spectra $R(\lambda)$ and the $(1-R(\lambda))$ of the Mo films on SS1, SS2 and SS3 substrates are shown in Figs. 6 and 10, respectively.

For the Mo/SS1 sample, due to the reflectance $R(\lambda)$ mainly keeps unchanged with wavelength, the $(1-R(\lambda))$ mainly keeps unchanged with wavelength. Eq. (9) is obtained according to Eq. (7) and Eq. (8), which calculates the emittance of the Mo/SS1 at temperatures from 25 °C to 400 °C. Therefore, the emittance of Mo/SS1 keeps unchanged with temperature.

$$\varepsilon_T = \int\limits_{1\mu m}^{100\mu m} (1 - R)I'_b(\lambda, T)\mathrm{d}\lambda = (1 - R)\int\limits_{1\mu m}^{100\mu m} I'_b(\lambda, T)\mathrm{d}\lambda = (1 - R)$$
$$= \text{constant} \tag{9}$$

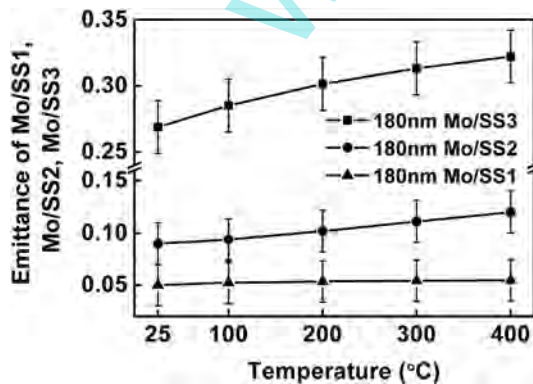For the Mo/SS2 and Mo/SS3 samples, the reflectance $R(\lambda)$

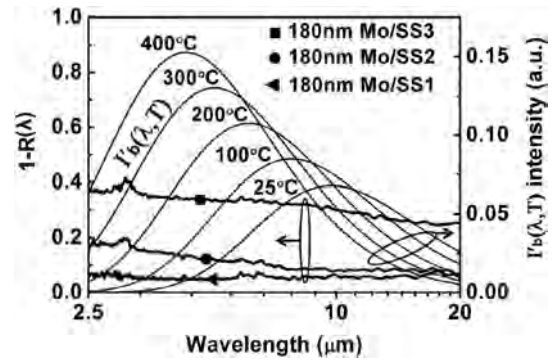Fig. 9. Emittance variation of the Mo films with temperature on SS1, SS2 and SS3 substrates.

Fig. 10. The $(1-R(\lambda))$ and $I'_b(\lambda, T)$ of the Mo films on SS1, SS2 and SS3 substrates.

increases with wavelength in Fig. 6. Because the action that increasing substrate surface roughness reduces the reflectance of the Mo film, is being weakened with increasing wavelength although the surface roughness value is fixed for the SS2 and SS3 substrates. Based on the variation of reflectance $R(\lambda)$ of Mo/SS2 and Mo/SS3, the $(1-R(\lambda))$ of them increases with decreasing wavelength, which results in larger values of $(1-R(\lambda))$ locating in the short wavelength range as shown in Fig. 10.

In Fig. 10, the integration of $I'_b(\lambda, T)$ being one represents the area under its curve. When the calculated temperature increases, the wave package (most of the area) of $I'_b(\lambda, T)$ is moving to the short wavelength range. And the main integral range of the emittance calculated at evaluated temperature is in the short wavelength range. According to Eq. (7) and Fig. 10, both larger $(1-R(\lambda))$ and $I'_b(\lambda, T)$ are in the short wavelength range and bring about larger emittance at evaluated temperature. Consequently, the emittance of Mo/SS2 and Mo/SS3 increases with temperature.

3.5. Mo/SS1 as IR-reflector for ZrSiON SSAC

The Mo/SS1 with the film thickness from 50 nm to 250 nm has the lowest thermal emittance 0.05 according to Fig. 5. And considering having both excellent thermal stability [33] and adhesion [34], the Mo/SS1 with an appropriate film thickness of 180 nm is chosen as the IR-reflector. The layer structure of the optimized SSAC of 61 nm SiO$_2$/23 nm ZrSiON/36 nm ZrSiN/180 nm Mo/SS1 is shown in Fig. 11. The reflectance spectra of the ZrSiON SSAC and the Mo/SS1 IR-reflector are shown in Fig. 12. The solar absorptance and thermal emittance of the SS1 substrate, Mo/SS1 IR-reflector and ZrSiON SSAC are listed in Table 3. The reflectance in solar radiation range is suppressed near zero after depositing the subsequent three layers of the ZrSiON SSAC on the Mo/SS1 IR-reflector. As a result, the solar absorptance increases to 0.92 from 0.34. The contributions of the increased absorption consist of three
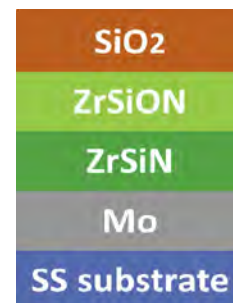

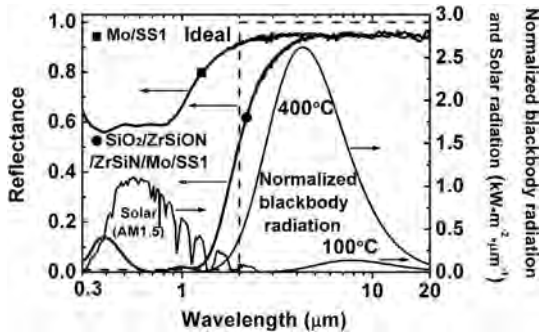Fig. 11. Schematic diagram of the SiO$_2$/ZrSiON/ZrSiN/Mo/SS SSAC.

Fig. 12. Reflectance spectra of the SiO$_2$/ZrSiON/ZrSiN/Mo/SS1 SSAC and the Mo/SS1 IR-reflector.

Table 3
The solar absorptance (α), thermal emittance (ε) of SS1 substrate, 180 nm Mo/SS1 IR-reflector and the optimal SiO$_2$/ZrSiON/ZrSiN/Mo/SS1 SSAC.

Samples	α	ε (100 °C)	ε (400 °C)
SS1 substrate	0.33	0.11	0.14
Mo/SS1	0.34	0.05	0.05
SiO$_2$/ZrSiON/ZrSiN/Mo/SS1	0.92	0.05	0.08

parts, which are the enhanced solar transmission by the SiO$_2$ anti-reflection layer, the intrinsic absorption by the ZrSiN layer and the interference absorption caused by the ZrSiON and ZrSiN layers.

The thermal emittance has been successfully decreased to 0.05 both at 100 °C and 400 °C from high values of 0.11 (100 °C) and 0.14 (400 °C) of the SS1 substrate by depositing the Mo film on it. The high IR reflectance of 0.95 in the wavelength range of 4–20 μm of the ZrSiON SSAC is guaranteed contributing to the high IR reflectance of the Mo/SS1 IR-reflector. As a result, the thermal emittance of the ZrSiON SSAC keeps 0.05 at 100 °C and increases to 0.08 at 400 °C. Owing to the high IR reflectance of the Mo/SS1 IR-reflector, the low thermal emittance of the ZrSiON SSAC is obtained. Therefore, the optimized Mo film shows an excellent property of high IR reflectance as an IR-reflector in SSAC.

4. Conclusion

In summary, the effects of the substrate material, substrate surface roughness, film thickness and temperature on the thermal emittance of Mo/substrate are discussed in this paper. The emittance of the Mo film is reduced by decreasing the substrate surface roughness. A saturated thickness 50 nm is found in the Mo films on glass (Sa = 3 nm), SS1 (Sa = 1 nm) and SS2 (Sa = 23 nm) substrates, but not on SS3 (Sa = 1497 nm) substrate. The thermal emittance of the Mo film on SS1 substrate keeps 0.05 from 25 °C to 400 °C, which satisfies the optical requirements for an IR-reflector. Based on the 180 nm Mo/SS1 IR-reflector, the optimized ZrSiON SSAC of 61 nm SiO$_2$/23 nm ZrSiON/36 nm ZrSiN/180 nm Mo/SS1 is prepared. The solar absorptance of the ZrSiON SSAC is 0.92 and the thermal emittance keeps 0.05 at 100 °C and increases to 0.08 at 400 °C. The results will provide valuable reference for choosing the surface morphology of the SS substrate and determining the film thickness of the metal IR-reflector layer properly, so as to keep the emittance of the metal layer as low as possible.

Acknowledgements

References

[1] C.E. Kennedy, Review of Mid- to High Temperature Solar Selective Absorber Materials, Technical Report, NREL/TP-520-31267, 2002.
[2] N. Selvakumar, Harish C. Barshilia, Review of physical vapor deposited (PVD) spectrally selective coatings for mid- and high-temperature solar thermal applications, Sol. Energy Mater. Sol. Cells 98 (2012) 1–23.
[3] J.X. Feng, S. Zhang, X. Liu, H.W. Yu, H.C. Ding, Y. Tian, J. Ouyang, Solar selective absorbing coatings TiN/TiSiN/SiN prepared on stainless steel substrates, Vacuum 121 (2015) 135–141.
[4] L. Cindrella, The real utility ranges of the solar selective coatings, Energy Mater. Sol. Cells 91 (2007) 1898–1901.
[5] H.D. Liu, Q. Wan, B.Z. Lin, L.L. Wang, X.F. Yang, R.Y. Wang, D.Q. Gong, Y.B. Wang, F. Ren, Y.M. Chen, X.D. Cheng, B. Yang, The spectral properties and thermal stability of CrAlO-based solar selective absorbing nanocomposite coating, Sol. Energy Mater. Sol. Cells 122 (2014) 226–232.
[6] J.X. Feng, S. Zhang, Y. Lu, H.W. Yu, L.M. Kang, X.Y. Wang, Z.M. Liu, H.C. Ding, Y. Tian, J. Ouyang, The spectral selective absorbing characteristics and thermal stability of SS/TiAlN/TiAlSiN/Si$_3$N$_4$ tandem absorber prepared by magnetron sputtering, Sol. Energy 111 (2015) 350–356.
[7] L.Q. Zheng, F.Y. Gao, S.X. Zhao, F.Y. Zhou, J.P. Nshimiyimana, X.G. Diao, Optical design and co-sputtering preparation of high performance Mo-SiO$_2$ cermet solar selective absorbing coating, Appl. Surf. Sci. 280 (2013) 240–246.
[8] Q.C. Zhang, High efficiency Al-N cermet solar coatings with double cermet layer film structures, J. Phys. D Appl. Phys. 32 (1999) 1938–1944.
[9] J.A. Thornton, Influence of apparatus geometry and deposition conditions on the structure and topography of thick sputtered coatings, J. Vac. Sci. Technol. 11 (1974) 666–670.
[10] J.A. Thornton, D.W. Hoffman, Internal stresses in titanium, nickel, molybdenum, and tantalum films deposited by cylindrical magnetron sputtering, J. Vac. Sci. Technol. 14 (1977) 164–168.
[11] D.W. Hoffman, J.A. Thornton, The compressive stress transition in Al, V, Zr, Nb and W metal films sputtered at low working pressures, Thin Solid Films 45 (1977) 387–396.
[12] P.M.P. Salomé, J. Malaquias, P.A. Fernandes, A.F. da Cunha, Mo bilayer for thin film photovoltaics revisited, J. Phys. D Appl. Phys. 43 (2010), 345501 (7pp).
[13] J.H. Scofield, A. Duda, D. Albin, B.L. Ballardb, P.K. Predecki, Sputtered molybdenum bilayer back contact for copper indium diselenide-based polycrystalline thin-film solar cells, Thin Solid Films 260 (1995) 26–31.
[14] Y.F. Xue, C. Wang, Y. Sun, W.W. Wang, Y.X. Wu, Y.P. Ning, Preparation and spectral properties of solar selective absorbing MoSi$_2$–Al$_2$O$_3$ coating, Phys. Status Solidi A 211 (2014) 1519–1524.
[15] L.Q. Zheng, F.Y. Zhou, X.G. Diao, Properties of infrared high reflectance Mo film for solar selective coatings by MF sputtering, Mater. Sci. Forum 743–744 (2013) 857–862.
[16] Z.B. Huang, W.C. Zhou, X.F. Tang, D.M. Zhu, F. Luo, Effects of substrate roughness on infrared-emissivity characteristics of Au films deposited on Ni alloy, Thin Solid Films 519 (2011) 3100–3106.
[17] K.P. Sibin, S. John, H.C. Barshilia, Control of thermal emittance of stainless steel using sputtered tungsten thin films for solar thermal power applications, Sol. Energy Mater. Sol. Cells 133 (2015) 1–7.
[18] Y.F. Xue, C. Wang, W.W. Wang, Y. Liu, Y.X. Wu, Y.P. Ning, Y. Sun, Spectral properties and thermal stability of solar selective absorbing AlNi–Al$_2$O$_3$ cermet coating, Sol. Energy 96 (2013) 113–118.
[19] L.Q. Zheng, F.Y. Zhou, Z.D. Zhou, X.W. Song, G.B. Dong, M. Wang, X.G. Diao, Angular solar absorptance and thermal stability of Mo–SiO$_2$ double cermet solar selective absorber coating, Sol. Energy 115 (2015) 341–346.
[20] J. Wang, B.C. Wei, Q.R. Wei, D.J. Li, Optical property and thermal stability of Mo/Mo–SiO$_2$/SiO$_2$ solar selective coating prepared by magnetron sputtering, Phys. Status Solidi A 208 (2011) 664–669.
[21] J.A. Thornton, A.S. Penfold, J.L. Lamb, Sputter-deposited Al$_2$O$_3$/Mo/Al$_2$O$_3$ selective absorber coatings, Thin Solid Films 72 (1980) 101–109.
[22] Q.C. Zhang, Y.B. Yin, D.R. Mills, High efficiency Mo-Al$_2$O$_3$ cermet selective surfaces for high-temperature application, Sol. Energy Mater. Sol. Cells 40 (1996) 43–53.
[23] S. Esposito, A. Antonaia, M.L. Addonizio, S. Aprea, Fabrication and optimisation of highly efficient cermet-based spectrally selective coatings for high operating temperature, Thin Solid Films 517 (2009) 6000–6006.
[24] J.A. Thornton, J. Tabock, D.W. Hoffman, Internal stresses in metallic films deposited by cylindrical magnetron sputtering, Thin Solid Films 64 (1979) 111–119.
[25] B. Chapman, Glow Discharge Process: Sputtering and Plasma Etching, John Wiley & Sons, New York, 1980.
[26] U.C. Nwaogu, N.S. Tiedje, H.N. Hansen, A non-contact 3D method to characterize the surface roughness of castings, J. Mater. Process. Technol. 213 (2013) 59–68.
[27] S.X. Zhao, Spectrally Selective Solar Absorbing Coatings Prepared by dc Magnetron Sputtering, PhD. Thesis, Uppsala University, Sweden, 2007, pp. 36–37. ISSN 1651–6214.
[28] S.X. Zhao, C.G. Ribbing, E. Wäckelgård, New method to optimize a solar

absorber graded film profile, Sol. Energy 78 (2005) 125—130.

[29] J. Müller, B. Rech, J. Springer, M. Vanecek, TCO and light trapping in silicon thin film solar cells, Sol. Energy 77 (2004) 917—930.

[30] J. Meier, J. Spitznagel, S. Faÿ, C. Bucher, U. Graf, U. Kroll, S. Dubail, A. Shah, in: Proceedings of the 29th IEEE Photovoltaic Specialists Conference, 2002, pp. 1118—1121. New Orleans, USA.

[31] S. Faÿ, S. Dubail, U. Kroll, J. Meier, Y. Ziegler, A. Shah, in: Proceedings of the 16th European Photovoltaic Solar Energy Conference, 2000, pp. 361—364. Glasgow, UK.

[32] K.S. Chou, Y.C. Lu, The application of nanosized silver colloids in far infrared low-emissive coating, Thin Solid Films 515 (2007) 7217—7221.

[33] F. Cao, D. Kraemer, T.Y. Sun, Y.C. Lan, G. Chen, Z.F. Ren, Enhanced thermal stability of W-Ni-Al$_2$O$_3$ cermet-based spectrally selective solar absorbers with tungsten infrared reflectors, Adv. Energy Mater. 5 (2015) 1401042.

[34] D. Sheeja, B.K. Tay, K.W. Leong, C.H. Lee, Effect of film thickness on the stress and adhesion of diamond-like carbon coatings, Diam. Relat. Mater. 11 (2002) 1643—1647.